

Research Article

Experimental Study and Seismic Response Evaluation of Chlorobutyl Rubber-Based Viscoelastic Dampers

Farnoosh Roshan-Tabari ¹, Hamid Toopchi-Nezhad ¹
and Ghodrattollah Hashemi-Motlagh ^{2,3}

¹Department of Civil Engineering, Razi University, Kermanshah 67149-67346, Iran

²Advanced Polymer Materials and Processing Lab (APLabUT), School of Chemical Engineering, College of Engineering, University of Tehran, Tehran, Iran

³Azmoon Dana Plastic Co., Polymer Testing and Research Lab, 3rd Sanaat Ave, Qalleh Hassan Khan, Tehran 31148-14738, Iran

Correspondence should be addressed to Hamid Toopchi-Nezhad; toopchi@gmail.com

Received 18 September 2023; Revised 22 December 2023; Accepted 30 December 2023; Published 19 January 2024

Academic Editor: Antonio Batista

Copyright © 2024 Farnoosh Roshan-Tabari et al. This is an open access article distributed under the Creative Commons Attribution License, which permits unrestricted use, distribution, and reproduction in any medium, provided the original work is properly cited.

Conventional viscoelastic devices often use high-damping elastomeric pads, typically made of patented formulations, that are bonded to steel plates. The response properties of these pads under cyclic shear deformations directly influence the load-deformation hysteretic response of the device. Chlorobutyl (CIIR) is a high-damping rubber commonly used in industrial applications. However, this study found that the damping properties of a typical CIIR rubber compound are insufficient for effective structural seismic mitigation at ambient temperatures above 0°C. The goal of this study was to develop a new composite of CIIR, referred to as modified CIIR, with improved damping properties and to compare its performance with that of the reference CIIR rubber. In the first phase of the experimental studies, the viscoelastic characteristics of the reference and modified CIIR rubber materials were evaluated using dynamic mechanical thermal analysis (DMTA) in tension mode. Prototype viscoelastic damper devices were then fabricated from both the reference and modified CIIR rubber materials and subjected to cyclic shear tests at room temperature and various loading frequencies. The results showed that the modified CIIR rubber exhibited significantly improved effective damping compared to the reference CIIR. The final component of this study involved investigating the seismic response of a 2D frame structure equipped with prototype dampers made from both reference and modified CIIR materials, using nonlinear time-history analyses. The analysis results indicated that the modified CIIR rubber can be effectively utilized in the seismic response mitigation of structures.

1. Introduction

Viscoelastic dampers serve as supplemental devices in structural engineering to reduce the seismic response of structures [1], diminish wind-induced vibrations [2], mitigate the seismic pounding of structures [3], or minimize floor diaphragm vibrations caused by live loads [4]. These dampers typically use one or more elastomeric pads composed of high-damping rubber with specially formulated properties [5]. When the structure experiences vibrations, the elastomeric pads undergo cyclic shear deformation and, owing to their inherently high damping characteristics,

dissipate a significant amount of structural vibration energy. By incorporating viscoelastic supplemental dampers, the effective stiffness of the structure increases in addition to its effective damping. The performance of dampers, concerning effective damping and stiffness, is generally influenced by factors such as strain amplitude, excitation frequency, and ambient temperature [6–9].

The high inherent damping of the elastomers utilized in viscoelastic dampers is attributed to the molecular structure of the base rubber and the combination of components within the rubber compound. In [10], the inherent damping of rubber compounds with various base rubbers including

polyethylene, polymethyl methacrylate, polypropylene, styrene-butadiene rubber (SBR), isobutylene-isoprene rubber (IIR), and urethane was investigated. The findings revealed that polyethylene and IIR (commonly known as butyl) rubbers exhibited higher effective damping than other rubbers. In the case of IIR, the damping property can be enhanced by incorporating miscible polymer oligomers such as polyisobutylene as an additional relaxation component [11]. Physical methods can also be employed to increase the effective damping of rubber. For instance, Ghotb and Toopchi-Nezhad [12] developed innovative precompressed viscoelastic dampers using chlorobutyl rubber (CIIR). The frictional resistance between the chain molecules of the rubber was elevated by precompressing the elastomeric pads. Consequently, the effective damping increases when the damper pads undergo shear strain, and the rubber molecules slide against one another. The influence of compressive load on rate-dependent high-damping rubber bearings has also been studied [13].

The inherent damping of rubber materials used in viscoelastic dampers can be enhanced by modifying their compound formulations [14]. As a suitable option, a compound comprising EPDM and butyl (IIR) rubbers, along with the addition of 20 parts of carbon black and 20 parts of paraffinic oil to achieve rubber with high inherent damping, has been proposed [15]. In a different approach, modified silica fume was utilized as an alternative reinforcing filler to enhance the damping properties of natural rubber [16]. To improve the energy dissipation capability of neat nitrile-butadiene rubber (NBR), various organic small-molecule modifiers (AO1035, AO60, and AO80) in different amounts were employed [17]. The incorporation of CIIR into a compound with EPDM as the base rubber effectively improved the thermal and mechanical properties of the resulting blend, resulting in increased inherent damping at room temperature. However, the inherent damping of the resultant composition did not surpass that of chlorobutyl alone [15, 18]. By adding aliphatic C5 and aromatic C9 resins to the components of the CIIR rubber, an increase in effective damping was observed [19]. Similarly, terpene resin has demonstrated effectiveness in regulating the glass transition and expanding the effective damping temperature range of CIIR [20]. The combination of CIIR and PVC in a multilayer configuration within the rubber compound enhances its effective damping over a wider temperature range [21]. The viscoelastic properties of a composition consisting of NBR and CIIR were investigated in the frequency range 10 to 105 Hz to evaluate the influence of the carbon black ratio on these properties [22]. A high-damping rubber combining CIIR, NBR, and neoprene, which exhibited excellent performance at ambient temperatures, was developed [23]. In a composite material composed of CIIR and piezoelectric ceramic (PZT), the damping properties were improved by converting mechanical energy from vibration into electrical energy using PZT [24].

Rubber materials generally exhibit high damping properties at temperatures corresponding to their glass transition, which typically fall within the range of -20°C to -100°C , depending on their molecular structure. However,

these damping properties decrease significantly at temperatures above 0°C . Therefore, an important objective for improving the viscoelastic properties of rubber is to enhance its inherent damping at ambient temperatures above 0°C . As previously mentioned, CIIR rubber is known to possess relatively high damping properties compared with other rubber types. Nevertheless, similar to many other rubbers, the inherent damping of CIIR diminishes significantly at temperatures above 0°C . The objectives of this study were to boost the inherent damping of CIIR over a wider temperature range by refining its compound composition and examining the seismic response mitigation performance of the modified rubber. This paper comprises the following sections: (i) a novel high-damping composite of CIIR rubber was developed, and its damping properties over a wide range of temperatures were evaluated using dynamic mechanical thermal analysis (DMTA) in tension mode; (ii) prototype viscoelastic dampers were fabricated and tested under cyclic shear loads at various shear deformations and loading frequencies to evaluate their mechanical and damping properties at room temperature; (iii) the seismic response of a frame structure equipped with a viscoelastic damper was evaluated using a set of nonlinear time-history analyses to examine the seismic response mitigation capability of the modified rubber; and (iv) discussion and conclusions. In all cases, the research results were compared with those of the reference CIIR rubber (i.e., the base rubber blend on which the modifications were made).

2. Modified Blend of Chlorobutyl Rubber

The elastomer formulations investigated in this study used chlorobutyl (CIIR) as the base rubber. Chlorobutyl rubber, which is known for its relatively high damping characteristics, has a wide range of applications in various industries. It is derived through the halogenation of butyl rubber. Butyl rubber possesses excellent resistance to weathering agents and demonstrates high resistance to the infiltration of air and water [25]. The introduction of halogens enhances the polymer chain flexibility of butyl rubber, thereby improving its compatibility with polar rubbers. Compared to butyl rubber, chlorobutyl rubber exhibits enhanced damping properties and shows superior bonding and compatibility with polar rubbers in the production of multirubber compounds [26].

The dynamic mechanical properties of elastomeric materials are influenced by various factors, including the excitation frequency, temperature, molecular structure of the base polymer, and chemical cross-linking systems utilized. Additionally, the presence of reinforcing fillers, such as different types of carbon black, significantly affects the physical properties and viscoelastic behavior of these materials. During cyclic deformation, the stress and strain exhibit a phase shift, represented by an angle δ ranging from 0 to $\pi/2$ rad. Material behavior is described by a complex elastic modulus consisting of real and imaginary components. The ratio between the imaginary and real components, often known as the loss factor or loss tangent ($\tan \delta$), represents the tangent of the phase angle δ [22].

Table 1 lists the components of the reference CIIR rubber compound used in this study. The compound was prepared by mixing all components, except for the curing agents, in a 60 cc internal mixer with Banbury-type rotors from Misagh Afzar (Tehran, Iran) at 60 rpm and 130°C for 10 min. After resting for one day at room temperature, the compounds were mixed with curing agents (sulfur and accelerators) in a lab-scale two-roll mill from Berstorff (Hannover, Germany) at room temperature for 10 min. The compounds were then molded into 2 mm thick sheets using a hot press at 100 bar and 160°C for 8 min for DMTA testing.

Compression set, tensile properties, and change in properties after ageing of the cured compounds are given in Table 2. As expected, compression set and tensile properties of modified CIIR are not as good as those of the reference CIIR due to the immiscibility of NBR, CIIR, and CPE in the blend of modified CIIR. To evaluate the stability of the compounds, the cured compounds were aged at 70°C for 168 h and the properties after ageing was measured. As seen, the mass of the compounds was nearly constant with less than 1% reduction showing the stability of the compounds via ageing. The tensile strength of the compounds was slightly increased while a small decrease was observed for the elongation at break. Overall, the properties of modified CIIR did not severely deteriorate with oven ageing. However, further improvement in the compatibility of CIIR/NBR is required.

The mechanical properties of rubber under dynamic loading were determined using DMTA tests with a Netzsch-DMA 242C instrument. This instrument can measure the mechanical properties of rubber under dynamic loading at various temperatures and frequencies. The test was conducted according to the ASTM D5026 standard [27], in which laboratory rubber samples were subjected to cyclic tensile stresses at two individual frequencies of 0.1 and 1 Hz. The temperature was varied from -100 to $+100$ °C at a heating rate of 3°C/min.

Figure 1(a) shows the variation in the loss factor ($\tan \delta$) of the reference CIIR with ambient temperature under cyclic tension at loading frequencies of 0.1 and 1.0 Hz. As seen in this figure, the loss factor ($\tan \delta$) of the reference rubber material increased with increasing loading frequency. At a loading frequency of 1 Hz, the rubber loss factor reached an absolute peak value of 1.35 at a temperature of -45 °C. As shown in Figure 1(a), the magnitude of $\tan \delta$ in the reference CIIR rubber reached 0.4 at 0°C and decreased significantly at temperatures above 0°C.

One way to enhance the damping properties of a rubber compound within a specific temperature range is to blend it with another rubber that exhibits its highest loss factor at a temperature higher than that of the base rubber. Nitrile butadiene rubber (NBR), detailed in Table 1, exemplifies such a rubber material. According to Figure 1(b), the rubber reaches an absolute peak value of ($\tan \delta$)=1.38 at approximately -13 °C, which is notably higher than the corresponding temperature for the reference CIIR. A comparison of Figures 1(a) and 1(b) reveals that damping properties of the NBR are more rate sensitive than those of the reference CIIR.

TABLE 1: Components of rubber formulations.

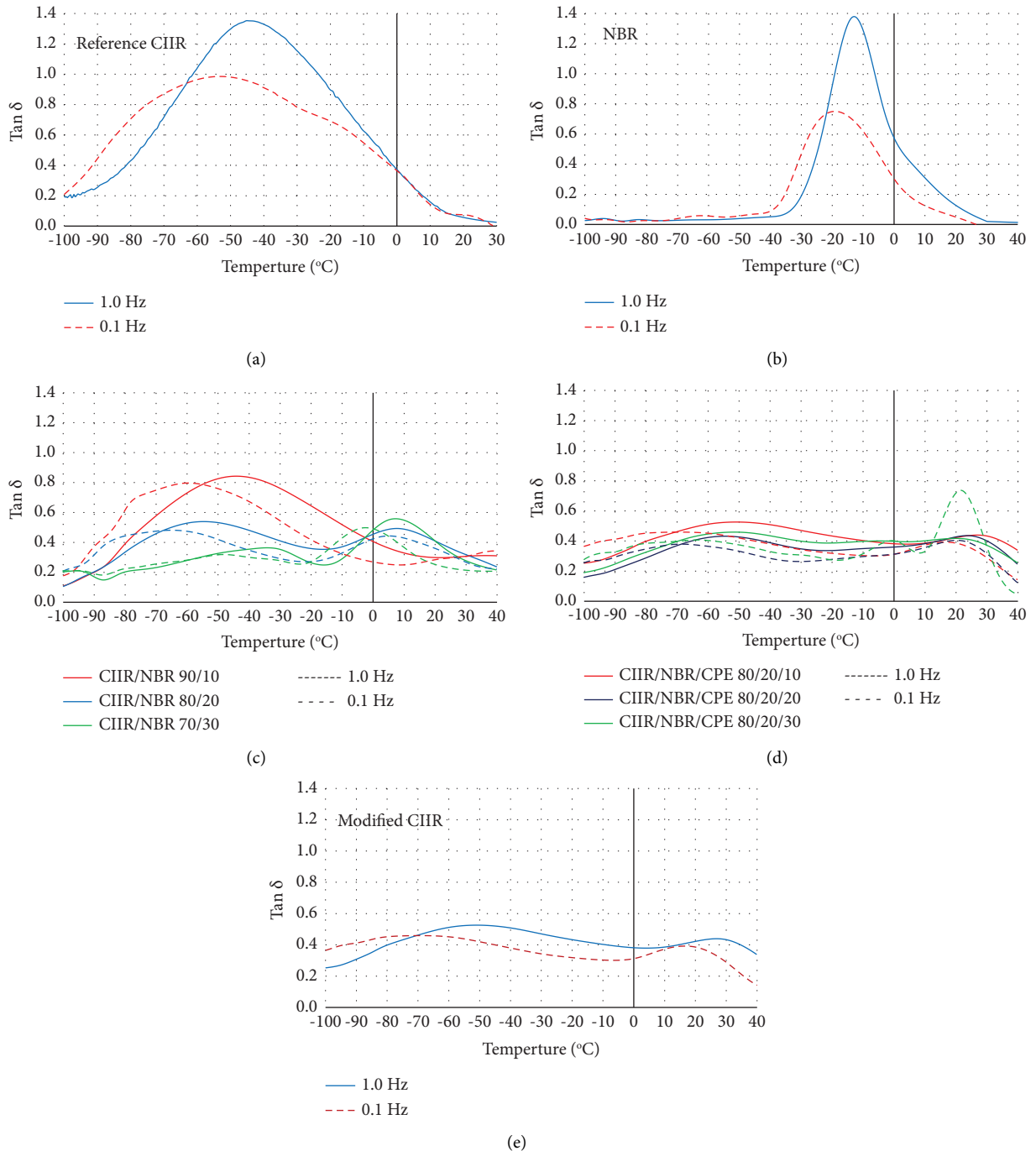
Ingredient (PHR)	Compound		
	Reference CIIR	NBR	Modified CIIR
CIIR	100	0	80
NBR	0	100	20
CPE	0	0	10
Carbon black	30	30	30
Sulfur	2	2	2
Paraffinic oil	20	20	20
Coumarone resin	3.5	3.5	3.5
ZnO	5	5	5
Stearic acid	1	1	1
Accelerators	3	3	3

Several rubber blends were created by combining different proportions of CIIR and NBR. Figure 1(c) displays the change in loss factor with temperature for these blends, with relative part ratios of CIIR/NBR at 90/10, 80/20, and 70/30. The tests were performed using two different excitation frequencies: 1.0 Hz (represented by the solid curve) and 0.1 Hz (represented by the dashed curve). Comparing Figures 1(a)–1(c), it can be observed that, in general, the loss factor of the CIIR/NBR blends increases when the temperature rises above 0°C. Based on Figure 1(c), it can be observed that in the CIIR/NBR blend with a part ratio of 90/10, the properties were predominantly governed by CIIR, as indicated by the occurrence of the highest peak loss factor at a significantly low negative temperature. Conversely, in the blend with a part ratio of 70/30, only a single peak loss factor was observed, and it occurred at approximately $+7$ °C. In the case of the 80/20 part ratio, two peak values were evident at around -55 and $+8$ °C when tested under an excitation frequency of 1.0 Hz. Additionally, the rate of change in the loss factor with temperature was relatively lower for the 80/20 part ratio compared to the other ratios. Based on these findings, the 80/20 part ratio was chosen as the focus of further research. Figure 1(c) reveals that this particular rubber blend exhibits a considerable 50% variation in the loss factor between its two peak values, indicating a significant effect. This phenomenon can be attributed to the differences in polar compatibility between the blended rubbers. Specifically, CIIR rubber possesses low polarity, whereas NBR displays high polarity [23].

Due to the significant polarity difference between CIIR (1.6 mol% chlorine) and NBR (33 mol% nitrile), this study incorporated chlorinated polyethylene (CPE) as an intermediate material to enhance their compatibility. Different amounts of CPE were added to the CIIR/NBR 80/20 rubber blend to assess the optimal formulation that achieves improved polar compatibility between the CIIR and NBR rubber components. Figure 1(d) shows the variation in the loss factor with temperature for various added parts of CPE, namely, 10, 20, and 30. An examination of this figure indicates that the CIIR/NBR/CPE part ratio of 80/20/10 resulted in a higher and more uniform loss factor between the two peak values. Moreover, an electron microscopy SEM image-assisted microscale examination of the rubber compositions revealed that the fracture surfaces between the

TABLE 2: Properties of the cured compounds.

Property	Method	Reference CIIR	Modified CIIR
Compression set at 25%, 23°C, 72 h (%)	ISO 815-1	15	26
Elongation at break (%)	ISO 37	762 ± 91	468 ± 28
Tensile strength at break (MPa)		7.0 ± 0.9	4.9 ± 0.7
Properties after ageing: 168 h, 70°C ISO 188			
Elongation at break (%)	ISO 37	720 ± 51	397 ± 11
Tensile strength at break (MPa)		8.1 ± 0.7	5.3 ± 0.4
Change in hardness (shore A)	ISO 48-2	+3	+5
Mass change (wt %)	ISO 188	-0.6	-0.5

FIGURE 1: Variations of the loss factor ($\tan \delta$) with temperature under cyclic tension loads of various frequencies: (a) reference CIIR; (b) NBR; (c) CIIR/NBR; (d) CIIR/NBR/CPE; (e) modified CIIR.

rubber phases became smoother and more continuous without cracks upon adding 10 parts of CPE [28]. Consequently, the CIIR/NBR/CPE part ratios of 80/20/10 were chosen as the optimal formula for the high damping rubber in this study. The formula for this novel compound, named modified CIIR, is presented in Table 1. This nomenclature indicates that the base rubber of the modified compound was CIIR.

Figure 1(e) illustrates the variation in the loss factor of the modified CIIR with the ambient temperature. As seen in Figure 1(e), the $\tan \delta$ curves for the modified CIIR had two peaks at both loading frequencies of 1.0 and 0.1 Hz. At a loading frequency of 1.0 Hz, the magnitudes of the two peaks were 0.52 (at -50°C) and 0.44 (at $+27^\circ\text{C}$), respectively. The peak value of the loss factor at a loading frequency of 0.1 Hz was 0.4, which occurred at 18°C . The minimum value of the loss factor within the positive temperature range occurs at a temperature close to zero. At 0°C , the loss factor decreased by an average of approximately 17% compared with its positive temperature peak value, indicating a relatively small variation in damping properties with temperature compared with the reference CIIR.

This section included the DMTA testing, in which rubber specimens were subjected to dynamic tension. In supplemental viscoelastic dampers, the rubber pads within the damper typically undergo cyclic shear deformations. To evaluate the mechanical behavior of rubber materials under cyclic shear loads, several prototype viscoelastic dampers were constructed using both reference and modified CIIR rubber materials. Details are presented in the following section.

3. Cyclic Shear Tests

3.1. Prototype Viscoelastic Dampers. In order to assess the shear load-deformation hysteresis curves of the rubber materials, two different types of prototype viscoelastic dampers with identical dimensions but varying rubber materials (reference CIIR and modified CIIR) were produced and labeled as the “reference damper” and “modified damper,” respectively. Figure 2 shows pictures of the prototypes created for this study, with two samples made for each damper type. The dimensions of the dampers were identical for both types, with the only difference being the type of rubber material used. As seen in Figure 2, each damper unit had two layers of rubber pads of 8 mm thickness that were vulcanized separately before being bonded to three metal sheets using a cold bonding agent. The thickness of all metal sheets was 14 mm. Threaded holes of 8 mm in diameter were drilled on opposite sides of the metal sheets to provide support for the external and internal plates of the dampers.

Figure 3(a) shows the assembly of the damper and the connection of the damper unit to the universal fatigue testing machine. An inner extending plate, A, was attached to the inner plate of the damper unit, whereas two outer extending plates (B) were connected to the outer plates of the damper unit via four bolts, D. To ensure that the damper unit was exposed to pure shear, plate C was introduced as an interface plate between outer plate B using two E bolts, perfectly aligned with plate A. The wedge grips (F) of the

testing machine were clamped to the roughened ends of plates A and C, and the tensile and compressive forces applied to the specimen via grip F were transformed into fully reversal cyclic shear forces on the rubber pads of the damper unit.

Figure 3(b) illustrates the image of one of the viscoelastic damper units connected to extending plates A and B, along with interface plate C. To simplify the assembly and disassembly process, a single set of plates, namely A, B, and C, was fabricated for all tests conducted in this study, as shown in Figure 3(b). Each prototype damper could be easily assembled in this setup and subjected to cyclic shear loading tests on the fatigue-testing machine. Owing to payload limitations of the test machine, the viscoelastic dampers used in this study were manufactured at a reduced scale of 1 : 5. It was assumed that by installing supplemental dampers, the structural performance would improve, limiting the story drift ratio to a maximum of 1% for the design basis earthquake (DBE) hazard level. Furthermore, it was assumed that the damper was mounted on rigid chevron bracing, ensuring that its deformation matched the story drift of the structure. For a typical full-scale story height of 3 m, the damper would experience a displacement amplitude of 30 mm at the DBE hazard level. This translates to a damper displacement of 6 mm at a scale of 1 : 5. Considering a limit of 75% shear strain for the rubber pads of the damper at this displacement level, the required thickness of the rubber pads was calculated as 8 mm. Therefore, the rubber pads within the damper were designed to have a thickness of 8 mm, as shown in Figure 2.

3.2. Test Protocol and Response Evaluation. Cyclic shear tests were conducted at room temperature to evaluate the shear force-deformation hysteresis loops of the damper specimens and to determine the effective stiffness and damping properties corresponding to various shear strain levels. Given a target displacement of 6 mm at the DBE hazard level, the test protocol included the following stages [29]:

- (i) 10 fully reversed load cycles with a displacement amplitude of 4 mm equivalent to 0.67 times the target displacement at the DBE hazard level
- (ii) 5 fully reversed load cycles with a displacement amplitude of 8 mm equivalent to 1.33 times the target displacement at the DBE hazard level
- (iii) 3 fully reversed load cycles with a displacement amplitude of 12 mm equivalent to 2 times the target displacement at the DBE hazard level

The time history of the sinusoidal input displacements, depicted in Figure 4, aligns with the loading protocol described earlier. These input displacements were imposed on the prototype dampers at varying frequencies during separate test runs. Following the completion of the cyclic tests, the shear force-displacement curves of the dampers were analyzed.

By employing the Kelvin-Solid model [7], the reaction force in a viscoelastic damper, denoted as $F(t)$, is determined by equation (1), considering the displacement $u(t)$ and velocity $\dot{u}(t)$.

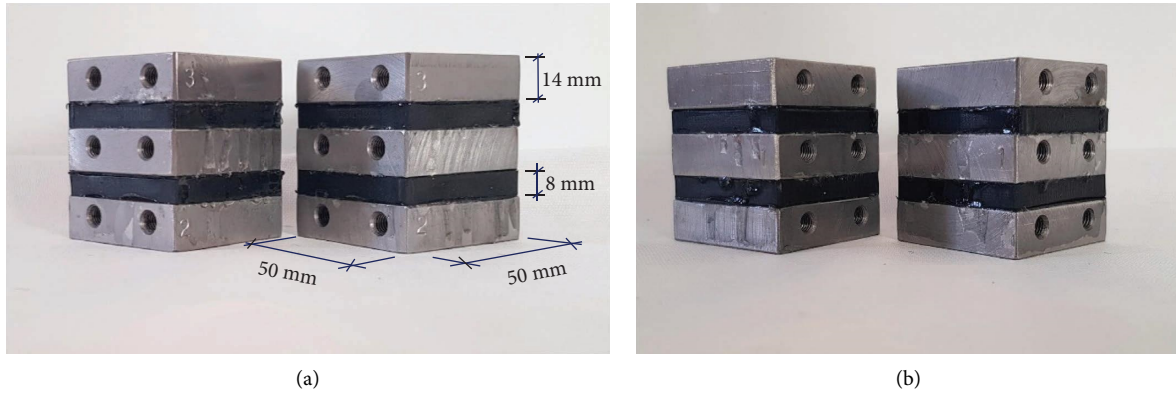


FIGURE 2: Damper units of various rubber pads: (a) Ref. CIIR pads; (b) Mod. CIIR pads.

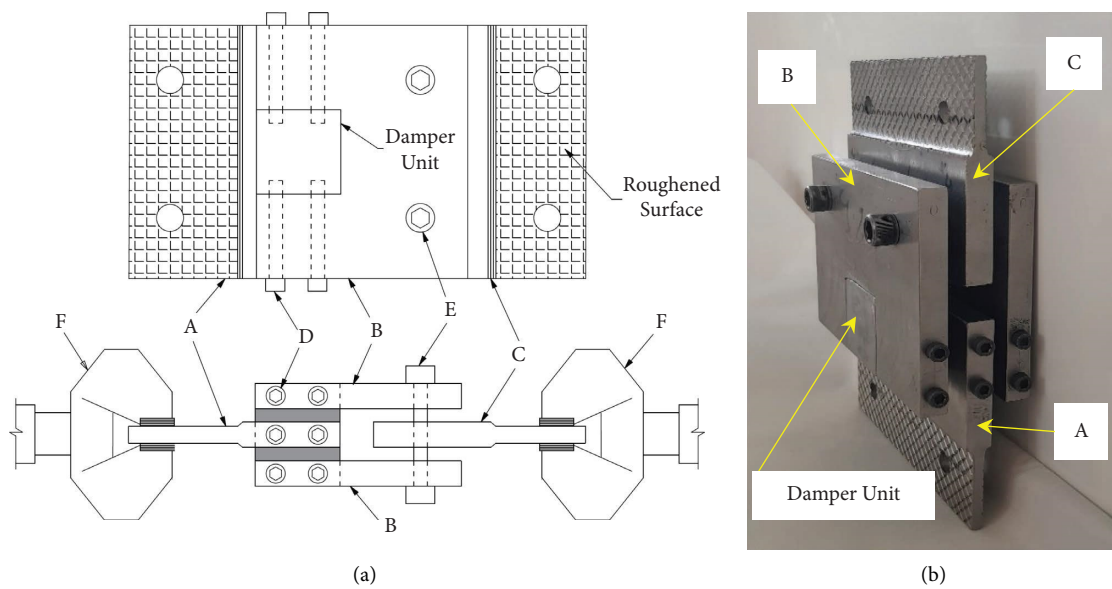


FIGURE 3: Prototype viscoelastic damper assembly: (a) sketch of components (plan and side views); (b) photo of the damper assembly.

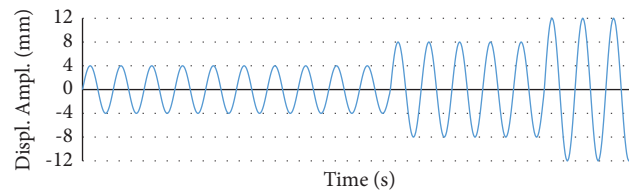


FIGURE 4: Time history of input displacements during cyclic shear testing.

$$F(t) = Ku(t) + C\dot{u}(t), \quad (1)$$

where K and C represent the effective (secant) stiffness and damping coefficient of the damper specimen, respectively. These parameters can be evaluated at each cycle of the tests as follows:

$$K = \frac{|F^-| + |F^+|}{|\Delta^-| + |\Delta^+|}, \quad (2)$$

$$C = \frac{W_D}{\pi \Delta_{ave}^2 \dot{\omega}}, \quad (3)$$

where F^- and F^+ represent the peak negative and positive forces resisted by the damper during the test cycle of negative and positive peak displacement amplitudes Δ^- and Δ^+ , respectively. Parameter W_D denotes the area enclosed by the force-displacement hysteresis curve obtained for the load cycle of interest. $\bar{\omega}$ represents the excitation frequency, and Δ_{ave} in each load cycle is calculated as follows:

$$\Delta_{ave} = \frac{|\Delta^-| + |\Delta^+|}{2}. \quad (4)$$

The equivalent viscous damping ratio of the viscoelastic prototype dampers, β , at each cycle of the test can be evaluated as follows:

$$\beta = \frac{1}{2\pi} \frac{W_D}{K\Delta_{ave}^2}. \quad (5)$$

3.3. Test Results and Discussion. Figure 5 shows the fatigue testing machine used for conducting cyclic loading tests on the prototype viscoelastic dampers employed in this study. This machine has a load capacity of 50 kN and can apply a maximum loading frequency of 100 Hz depending on the displacement amplitude of the load cycles. To adhere to the payload capacity of the test machine, the sinusoidal displacements outlined in Figure 6 were applied at frequencies of 0.5, 0.7, 1, and 3 Hz with target displacement amplitudes of 4, 8, and 12 mm. Owing to the limitations of the test machine, it was necessary to apply displacement cycles of the same amplitude individually to the test specimens as it was not feasible to execute load cycles of varying displacement amplitudes within a single test run. The test machine was capable of real-time measurement of the axial force and relative displacements between its two jaws. The outputs of the load cell and displacement transducers were recorded using a dynamic data logger at a frequency rate of 50 Hz. All tests were conducted at room temperature (24°C).

The graphs in Figure 6 show the shear force-deformation hysteresis loops of the prototype dampers. These dampers were tested under shear loading cycles at different excitation frequencies ranging from 0.5 Hz to 3 Hz. However, for the 3 Hz frequency, the testing machine had a limitation on the maximum displacement amplitude of 12 mm. Therefore, the damper specimens were loaded only within the range of 4–8 mm at this frequency.

The second specimen of each damper type yielded similar results to those of the first specimen when tested under cyclic shear conditions. Dynamic response parameters, such as the effective stiffness, damping coefficient, and equivalent viscous damping ratio, were evaluated for both specimens of each damper type. The variations in these parameters were less than 10%, indicating the repeatability of the dynamic response characteristics for each damper type. After each test run, the damper specimens were visually inspected to check for any physical damage. No significant physical damage was detected in the damper specimens during testing.

As shown in Figure 6, the damper utilizing the modified CIIR rubber material exhibited a significantly higher reaction force and a larger area enclosed by the force-

deformation hysteresis loops than the reference damper at all excitation frequencies. This increase in the reaction force indicated an improvement in the effective stiffness of the damper during each test cycle. Additionally, the larger enclosed area of the hysteresis loops suggests that the modified damper has superior energy dissipation capability.

Table 3 includes the average stiffness, k , damping coefficient, c , and equivalent viscous damping ratio, β , evaluated for the 1/5 scale prototype dampers at various excitation frequencies, f .

Examining the data presented in Table 3, it is evident that the prototype damper incorporating the modified CIIR rubber material exhibits a significant increase (at least 100%) in effective stiffness compared to the prototype damper made with the reference CIIR. In both types of rubber, the effective stiffness decreased as the shear deformation increased at a constant excitation frequency. This behavior aligns with the findings of previous studies, such as [30]. The rate of decrease in the effective stiffness with increasing shear deformation was similar for both the reference and modified CIIR materials. When the shear deformation tripled (from 4 to 12 mm), the effective stiffness of the dampers decreased by approximately 30%.

Based on the data presented in Table 3, the effective stiffness generally increases as the excitation frequency increases. The effect of the excitation frequency on the effective stiffness of the rubber materials was not significant at deformations of 4 and 8 mm, up to a frequency of 1 Hz. However, at a shear deformation of 12 mm, the influence of the excitation frequency became more noticeable. In this deformation range, the damper stiffness increased by 32% for the reference CIIR and by 37% for the modified CIIR when the excitation frequency was increased from 0.5 Hz to 1 Hz. The stiffness of the modified CIIR increases significantly at a loading frequency of 3 Hz. Specifically, at a shear deformation of 4 mm, the stiffness of the modified CIIR increases by approximately 16%. However, there was no significant variation in the stiffness of the reference CIIR at an excitation frequency of 3 Hz compared with the previous lower frequencies.

By comparing the damping coefficients, c , of the rubber materials listed in Table 3, it is evident that the modified CIIR exhibits a significant increase (at least 160%) in its damping coefficient compared to the reference CIIR. On average, the modified CIIR exhibited an equivalent viscous damping ratio approximately 50% higher than that of the reference CIIR. Furthermore, when compared to the reference CIIR, the damping ratio of the modified CIIR was found to be relatively more responsive to changes in excitation frequency. The damping ratio exhibited minimal variations with respect to the shear deformations. In general, the damping ratio of the examined rubber materials varied within $\pm 15\%$ when compared to an excitation frequency of 0.5 Hz. Notably, the modified CIIR material exhibited the highest damping ratio at an excitation frequency of 3 Hz.

The hysteresis loops of the cyclic shear load deformation offer valuable insights into the dynamic response characteristics of damper devices. In the following section, the seismic mitigation efficiency of the corresponding full-scale model of the dampers is examined using nonlinear time-history analyses.

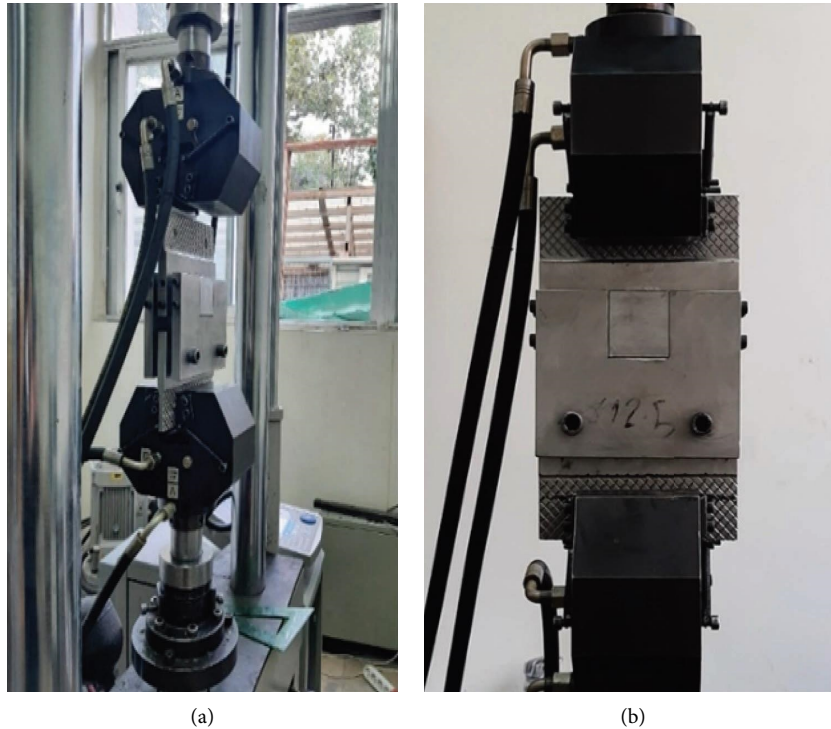


FIGURE 5: Cyclic shear test setup: (a) installation of damper specimen in test machine; (b) front view of damper under cyclic loading.

4. Seismic Response Assessment

The primary aim of this section is to comprehensively evaluate, compare, and assess the seismic response of a case study frame structure equipped with both reference and modified viscoelastic dampers. The response was evaluated using a series of nonlinear time-history analyses.

4.1. Case Study Structure. The case study structure used in this research was a 2D single-story steel moment-resisting frame with four bays, each having an equal span of 5 m and a story height of 3 m. This case study structure is hereafter referred to as the original frame (OF). Refer to Figure 7(a) for the frame geometry and designated W-sections for each beam and column in the stick model developed in SAP2000 [31]. The total mass of the structure was 75 t, and its fundamental natural frequency was determined to be 0.84 Hz. The frame exhibits an inherent damping ratio of 5%. The A36 steel material was assumed for all structural elements, considering the default stress-strain plot and property data of SAP2000 [31], which were employed in the nonlinear time-history analysis of the frame structure.

Figure 7(b) illustrates the retrofitted frame, which includes a viscoelastic supplemental damper installed on rigid chevron bracing. To compare the seismic response mitigation achieved by the different dampers in this study, the frame structure was equipped with each of the reference and modified viscoelastic dampers separately. The original frame (OF) retrofitted with the reference damper (RD) is referred to as OF + RD, whereas the frame retrofitted with the modified damper (MD) is denoted as OF + MD.

In a simplified approach, the viscoelastic damper in SAP2000 was modeled using a link element. This element consists of a linear spring (k) and linear dashpot (c) connected in parallel (Figure 7(b)). The parameters k and c for both the reference and modified viscoelastic dampers were determined based on cyclic shear tests performed on their 1/5 scale prototype dampers. The results of these tests are presented in Table 4.

According to the dynamic similitude law, in a true replica model, the full-scale values of f , k , and c are evaluated by multiplying their model-scale quantities by $1/\sqrt{s}$, s , and $\sqrt{(s^3)}$, respectively [32]. In this study, the scale factor s was set to 5. It should be noted that because the fundamental frequency of the original frame and its retrofitted versions exceeds 0.84 Hz, Table 3 provides the corresponding full-scale response values of the dampers at excitation frequencies of 0.45 Hz and 1.34 Hz only. These frequencies bracket the frequency of the original frame, which was 0.84 Hz.

The final values for k and c of the damper in the time-history analysis are determined through an iterative process based on the peak story drift and fundamental frequency of the retrofitted frame, as they are dependent on the rate and amplitude. The fundamental frequencies of the OF + RD and OF + MD systems based on the initial stiffness of the dampers were calculated to be 1.08 Hz and 1.34 Hz, respectively. These frequency values fell within the range of 0.45 to 1.34 Hz as shown in Table 4. As a result, the damper response properties can be evaluated by linear interpolation between the f values of 0.45 and 1.34 Hz. For the OF + MD system, the response properties at the frequency of 1.34 Hz were used (see Table 4).

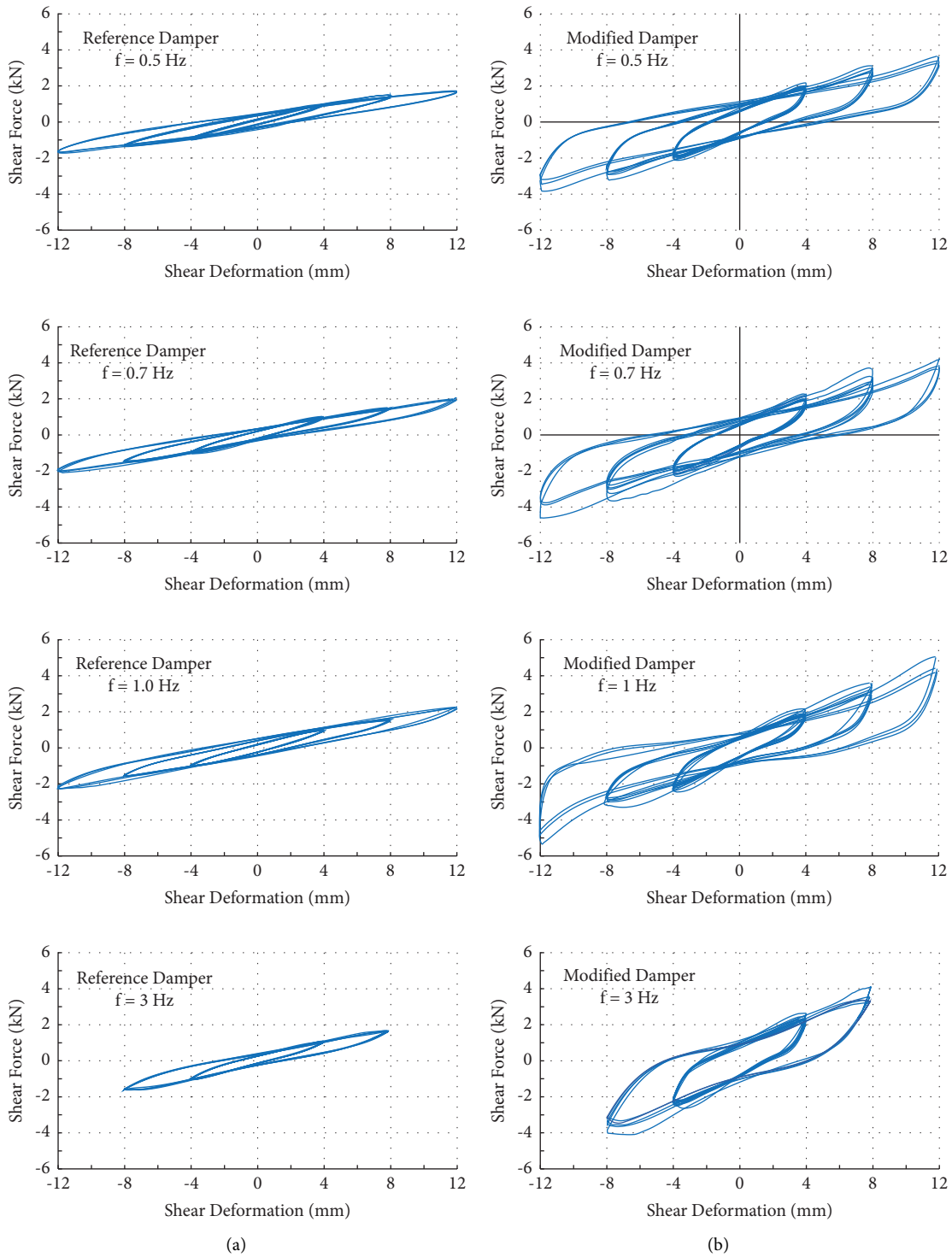


FIGURE 6: Cyclic load-displacement hysteresis loops of the damper specimens at various excitation frequencies: (a) reference damper (Ref. CIIR); (b) modified damper (Mod. CIIR).

As mentioned previously, the properties of the damper are influenced by the amplitude of the deformations imposed on it. According to Figure 7(b), which shows the damper configuration, the damper deformation is equal to the lateral displacement x imposed on the frame structure. Figure 8 illustrates how damper parameters k and c vary with

displacement x . The data points of this curve were calculated from Table 4 by using linear interpolation based on the frequency f of the retrofitted frame. As shown in Table 4, at an excitation frequency of 1.34 Hz, only two data points exist at displacements of 20 and 40 mm. This was due to the payload limitation of the test machine, which could not

TABLE 3: Experimentally evaluated response properties of the 1/5 scale prototype viscoelastic dampers.

f (Hz)	Shear deformation (mm)	Reference CIIR			Modified CIIR		
		k_0 (kN/mm)	c_0 (kN.s/mm)	β_0	k (kN/mm)	c (kN.s/mm)	β
0.5	4	0.239	0.0108	0.07	0.574	0.0641	0.18
	8	0.172	0.0124	0.11	0.461	0.0525	0.18
	12	0.144	0.0115	0.12	0.369	0.0372	0.16
0.7	4	0.255	0.0128	0.11	0.537	0.0461	0.19
	8	0.196	0.0111	0.12	0.396	0.0325	0.18
	12	0.189	0.0094	0.11	0.312	0.0247	0.17
1.0	4	0.259	0.0097	0.12	0.576	0.0275	0.15
	8	0.190	0.0064	0.11	0.428	0.0217	0.16
	12	0.173	0.0054	0.10	0.433	0.0187	0.14
3.0	4	0.261	0.0031	0.11	0.659	0.0155	0.22
	8	0.206	0.0027	0.12	0.518	0.0105	0.19

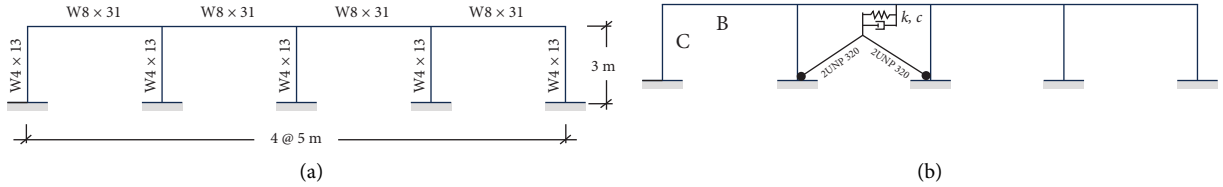


FIGURE 7: Moment-resisting frame structure: (a) original frame; (b) retrofitted frame.

handle cyclic shear tests on 1/5 scale prototype dampers with a displacement amplitude of 12 mm at a loading frequency of 3 Hz. Because the variation of k and c with x is nonlinear by nature (see Figure 8(a)), the third data point in each diagram in Figure 8(b) was generated to maintain the same response reduction achieved between the third and second data points in Figure 8(a)'s k and c parameters. The equation of a curve fitted to each case's data points is used to establish a mathematical relationship between the damper parameters k and c and displacements x . During each iteration of the time-history analysis, the k and c values were updated based on the peak displacement, x , imposed on the damper. The iterations continued until the damper's peak displacement converged to its unique value with an error of 1%.

4.2. Earthquake Events. Table 5 presents the earthquake events selected for the time-history analyses of this study. These earthquakes were far-field events, all recorded on site class D, which represents stiff soil [33]. The peak ground accelerations of these earthquakes were scaled to 0.5 g. In practical design applications, it is crucial to adjust the ground acceleration records to align them with the design response spectrum, particularly around the fundamental period of the structure. This spectrum is derived from earthquake hazards and soil conditions. Despite this, the current study did not factor in a specific site location or corresponding design response spectrum. As a result, the earthquakes' peak ground acceleration (PGA) was adjusted to 0.5 g. This adjustment enabled a standardized comparison of the seismic response of the frame structure under a uniform intensity measure. The input earthquakes in this

study represent severe events that are comparable to the maximum credible earthquake (MCE) hazard level. Despite the presence of the damper and response mitigation achieved, the structure may undergo significant drift ratios, suggesting that its structural elements are subject to nonlinear deformations. Consequently, in the time-history analyses, the inherent damping of the frame structure was assumed to be 5%.

To gain a better understanding of the frequency content of earthquakes, their power spectral density (PSD) plots are illustrated in Figure 9. As shown in this figure, the power spectrum of the Scaled Bam earthquake has a peak at a frequency of 0.83 Hz, which closely matches the fundamental frequency of the original frame. Consequently, this earthquake is expected to be a challenging event for the original frame, causing resonance excitation. The power spectrum of the Scaled Northridge earthquake has two initial peaks at frequencies of 0.58 and 1.66 Hz, which encompassed the fundamental frequencies of all three frame structures. The power spectrum of the Scaled Tabas had a peak at the natural frequency of the OF + MD system, which was 1.34 Hz. Consequently, this earthquake is expected to be a challenging event for this structural system.

4.3. Seismic Analysis Results and Discussion. Nonlinear time-history analysis was performed on the frame structures using each of the input earthquakes listed in Table 5. To assess the dampers' impact on the frame's dynamic response, the energy components (shown in Figure 10) and the roof displacement history (shown in Figure 11) were evaluated and examined.

TABLE 4: Response properties of full-scale prototype viscoelastic dampers.

f (Hz)	Displacement (mm)	Reference damper		Modified damper	
		k_0 (kN/mm)	c_0 (kN.s/mm)	k (kN/mm)	c (kN.s/mm)
0.45	20	1.294	0.1084	2.880	0.3075
	40	0.947	0.0712	2.140	0.2426
	60	0.865	0.0599	2.165	0.2091
1.34	20	1.304	0.0347	3.294	0.1733
	40	1.032	0.0301	2.588	0.1174

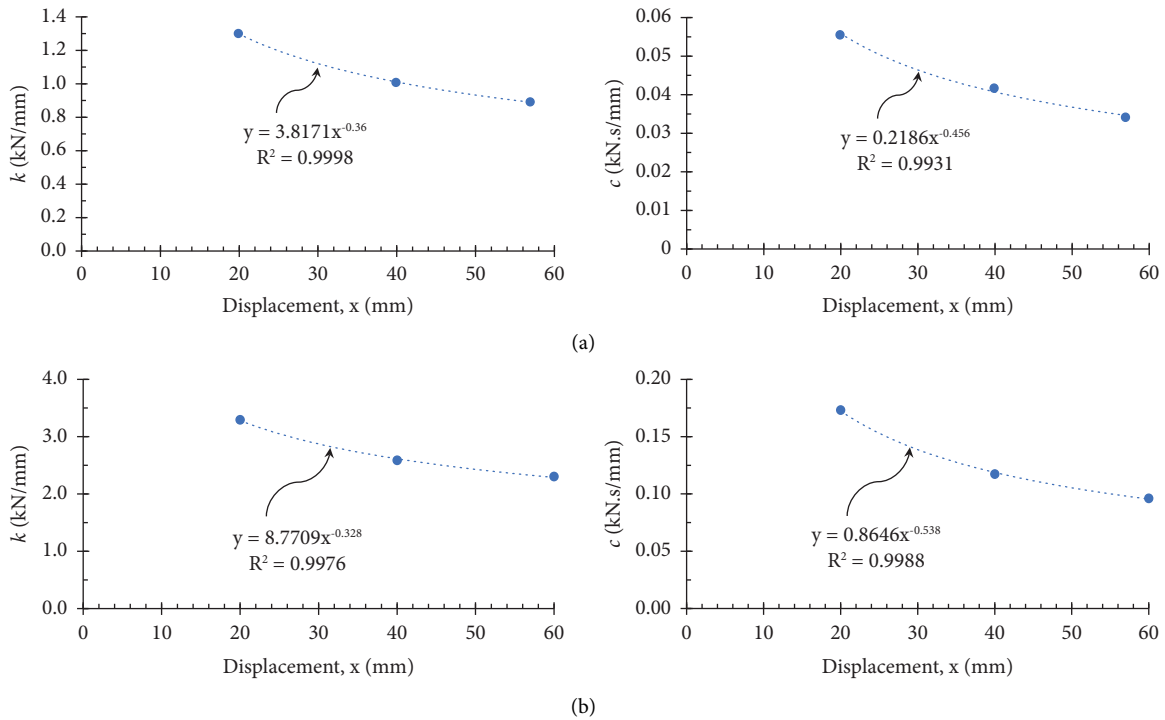


FIGURE 8: Variation of k and c of the viscoelastic dampers with lateral displacements: (a) reference damper, $f = 1.08$ Hz; (b) modified damper, $f = 1.34$ Hz.

TABLE 5: Earthquake events used for time-history analysis.




Earthquake name	Year	Station name	Magnitude	Scaled accelerogram
Tabas	1978	Ferdows	6.40	
Northridge	1994	LA-Century City CC North	6.69	
Bam	2003	Golbaf 1	6.50	

Figure 10 displays the cumulative plot of the earthquake input energy, the structure’s modal energy, and the energy dissipated by the supplemental viscoelastic damper in the different frame structures. The cumulative modal energy

represents the total energy accumulated in the vibration modes of the structure during an earthquake. By reducing this energy, the response of the structure to seismic forces can be minimized, resulting in improved performance and reduced damage.

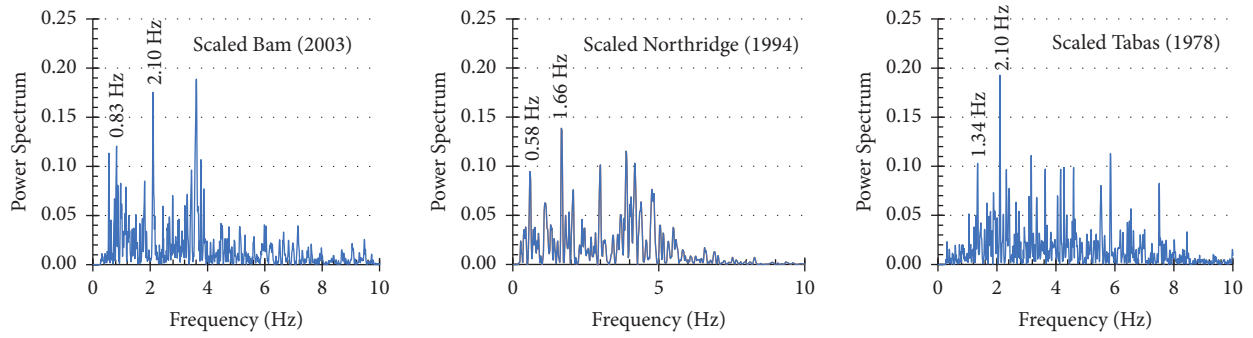


FIGURE 9: Power spectrum of the scaled earthquakes.

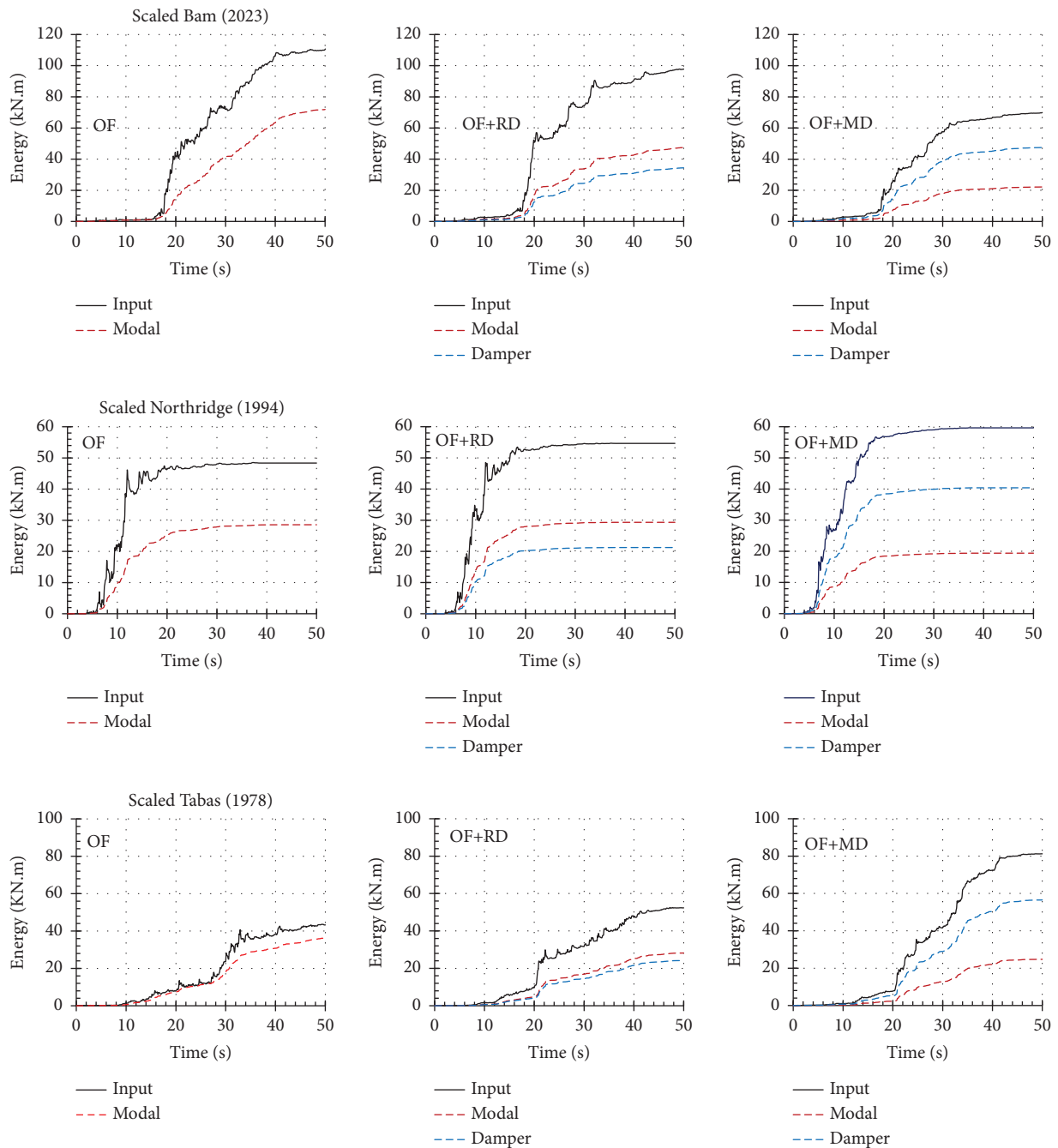


FIGURE 10: Cumulative energy plots under different earthquakes for the OF, OF + RD, and OF + MD systems.

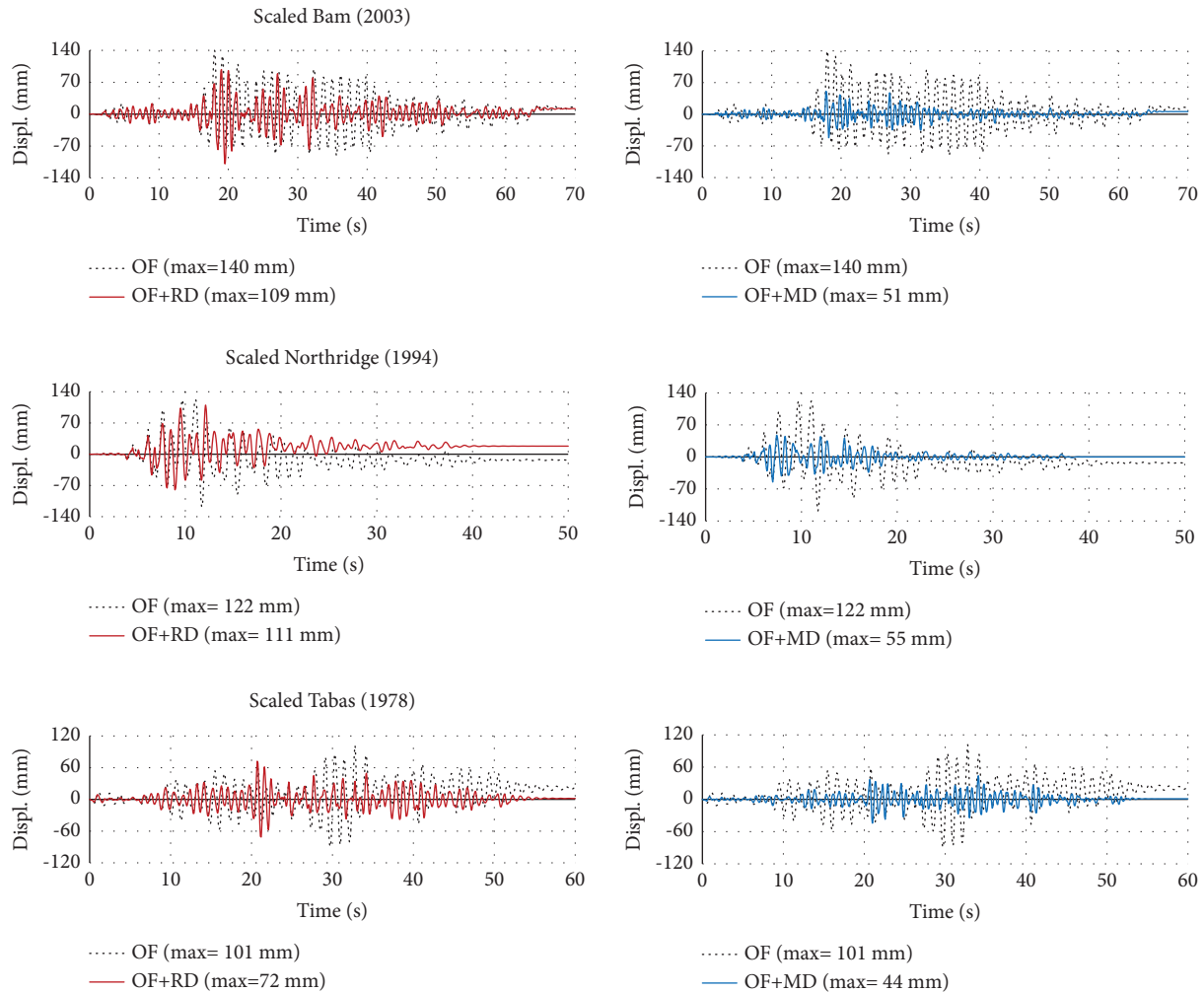


FIGURE 11: Time history of roof displacement in ordinary frame (OF), frame equipped with reference damper (OF + RD), and frame equipped with modified damper (OF + MD) under various earthquakes.

4.3.1. Response to the Scaled Bam Earthquake

(i) *Energy flow to structures*: As mentioned in the previous section, the frequency content of the Scaled Bam earthquake causes resonance in the OF structure. According to Figure 10, this earthquake had the highest energy input to the OF structure among the other three earthquakes, with a significant portion of the input energy being transferred into modal energy. When comparing the plots of modal energies during the other earthquakes, it is clear that the Scaled Bam earthquake is the most devastating for the OF structure. However, by adding a supplemental viscoelastic damper, the stiffness and effective damping of the OF structure increased, shifting its fundamental frequency beyond the resonance region and reducing its seismic response. As shown in Figure 10, both the reference and modified dampers reduced the input energy to the structure and its modal energy during the Scaled Bam earthquake. Owing to its relatively low inherent damping, the reference damper absorbed less energy

than the modal energy. Nonetheless, the reference damper resulted in a reduction of approximately 35% in the cumulative modal energy compared to the OF structure. In contrast, in the OF + MD system, a significant portion of the energy input to the structure was dissipated by the supplemental damper, reducing its modal energy by approximately 70% compared to the OF structure, indicating a significant response mitigation.

(ii) *Roof displacements*: Figure 11 illustrates that the OF structure experienced its maximum lateral displacement during the Scaled Bam earthquake, with a drift ratio of 4.7%, significantly exceeding the maximum tolerated value of 2.5% specified by current design codes such as ASCE/SEI 7 [33]. The reference damper reduced the peak lateral displacement by 22%; however, this response mitigation was insufficient as the drift ratio remained beyond the permissible limit. Additionally, the maximum displacement experienced by the reference damper is 109 mm, significantly larger than its

displacement capacity of 60 mm as specified in Table 4. In contrast, the application of the modified damper in the OF + MD system resulted in an approximately 64% decrease in the peak lateral displacement compared with the OF structure, which is significant. The peak drift ratio of the frame structure was limited to a tolerable amount of 1.7% for risk categories I, II, and III [33], and the damper displacements remained within the permissible range of 0–60 mm. The definition of risk categories of buildings and other structures for extraordinary loads and events including earthquakes according to ASCE 7 [33] is given in Table 6.

4.3.2. Response to the Scaled Northridge Earthquake

- (i) *Energy flow to structures*: During the Scaled Northridge earthquake, the OF + MD system experienced the highest input energy and lowest modal energy (see Figure 10). In this system, the modal energy decreased by approximately 32% compared with the OF structure, indicating the significant contribution of the modified damper in dissipating the input energy of the earthquake. In contrast, in the OF + RD system, the input energy to the structure increased by approximately 13% compared with the OF structure, and both systems had almost the same modal energy. The reference damper did not noticeably reduce the structural response.
- (ii) *Roof displacements*: During the Scaled Northridge earthquake, the peak drift ratio of the OF structure reached 3.4%, exceeding the maximum permissible limit mandated by the ASCE 7 code. The reference damper in the OF + RD system mitigated the drift ratio by 2.4%, which was acceptable for risk categories I and II [33]. In contrast, in the OF + MD system, the drift ratio was limited to 1.5%, which is the permissible limit for all risk categories, including risk category IV [33]. This indicates the adequate performance of the modified damper in mitigating the frame structure response to the Scaled Northridge earthquake.

4.3.3. Response to the Scaled Tabas Earthquake

- (i) *Energy flow to structures*: As mentioned earlier, one of the dominant frequencies of the Scaled Tabas earthquake was in harmony with the fundamental frequency of the OF + MD system. This resulted in the highest input energy to the system during an earthquake. Compared with the OF structure, the energy input to the OF + MD system increased by approximately 86%. However, the modified damper dissipated a significant amount of this input energy (see Figure 10, Scaled Tabas, OF + MD). The cumulative amount of modal energy in this system

reached approximately 67% of the modal energy of the OF structure, which had a significantly lower input energy. This demonstrates the effectiveness of the modified damper in mitigating the seismic response of the frame structure even when its response is at resonance. In this earthquake, as with the other two earthquakes, the reference damper was unable to overtake the modal energy of the structure, indicating unsatisfactory performance.

- (ii) *Roof displacements*: Similar to previous earthquakes, the drift ratio of the OF structure exceeds the permissible limit specified by the code. The reference damper was subjected to lateral displacements beyond its displacement capacity and was at risk of damage. In contrast, the performance of the modified damper is satisfactory because it limits the drift ratio to 1.8%, a value tolerated for risk categories I to III [33].

Figures 12 and 13 show the maximum internal forces experienced by beam B and column C, respectively, which serve as representative structural elements of the frame structure, under various input earthquakes. The specific beam B and column C can be seen in Figure 12. Upon examining Figures 12 and 13, it becomes apparent that the introduction of the reference damper in the OF + RD system does not have a significant impact on overall response mitigation. In Figure 12, the modified damper reduces the shear and bending moments in beam B by at least 5% and 12%, respectively. Figure 13 shows that the axial load in the column is reduced by 6% in the OF + MD system compared with the uncontrolled OF system. It should be noted that a significant portion of the axial force in the column was caused by gravity loads. The modified damper led to a substantial decrease in the shear and bending moments in column C, with the internal shear load demand decreasing by at least 31%. While plastic hinges were formed in both the OF structure and the OF + RD system during all earthquakes, the bending moment in the OF + MD system was reduced by at least 30% when compared to the OF structure. Consequently, the application of the modified damper prevented the formation of plastic hinges in column C.

As only three earthquake records were selected to assess the response history of the structures, the performance of each damper was evaluated based on the minimum seismic mitigation achieved. Based on this evaluation, the reference damper in the OF + RD system was considered unsatisfactory. The reference damper failed to prevent the formation of plastic hinges in the columns and limited the frame structure drift ratio. Furthermore, it is prone to significant damage, as it experiences displacement beyond its capacity. On the other hand, the modified damper in the OF + MD system performed satisfactorily. The modified damper significantly reduced the modal energy, mitigated the internal forces, and prevented the formation of plastic hinges on the columns. Additionally, it limits the drift ratio to 1.8%, which is deemed acceptable for risk categories I–III, as defined in [33].

TABLE 6: Risk category of buildings and structures for earthquake loads [33].

Use or occupancy	Risk category
Buildings and other structures that represent low risk to human life in the event of failure	I
All buildings and other structures except those listed in risk categories I, III, and IV	II
Buildings and other structures (excluding essential facilities), the failure of which could pose a substantial risk to human life	III
Buildings and other structures designated as essential facilities, the failure of which could pose a substantial hazard to the community	IV

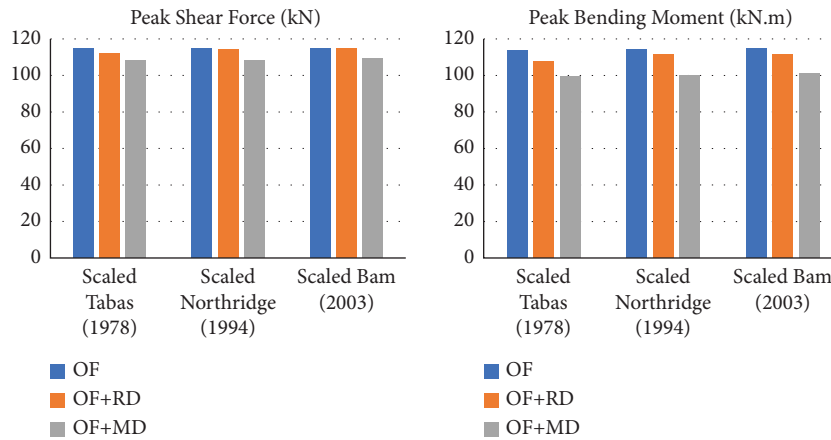


FIGURE 12: Peak demand internal forces in beam B.

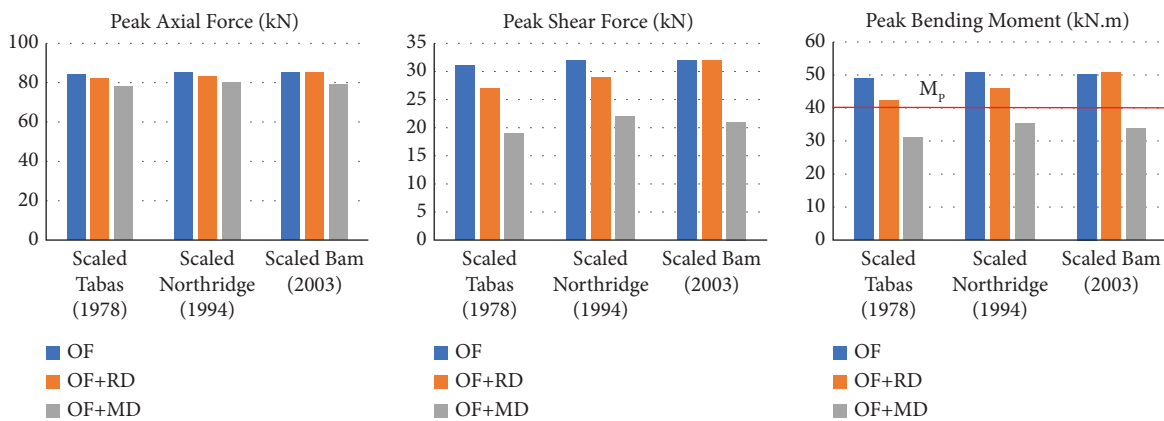


FIGURE 13: Peak demand internal forces in column C.

5. Summary and Conclusions

The primary objective of this study was to enhance the damping properties of a chlorobutyl (CIIR) rubber compound under low excitation frequencies at room temperature. To achieve this, the original CIIR compound (called reference rubber) was modified by blending it with neat nitrile-butadiene rubber (NBR) and chlorinated polyethylene (CPE) in a new formula, resulting in a novel compound known as the modified CIIR rubber. The study yielded several significant findings, as outlined below.

- (1) Dynamic mechanical thermal analysis (DMTA) tests:
 - (a) The reference rubber demonstrated its highest loss factor, $\tan \delta$, within a relatively limited temperature range of -45°C to -50°C . However, the loss factor decreases significantly outside this temperature range.
 - (b) The modified rubber exhibited an enhanced loss factor over a wide temperature range. The graph depicting the relationship between the loss factor and ambient temperature revealed two peaks of

nearly equal magnitude, occurring at -50°C and $+27^{\circ}\text{C}$. Throughout this temperature range, the rubber material demonstrated a more consistent $\tan \delta$, with a maximum variation of -20% compared to its highest value of 0.5.

(2) Cyclic shear tests:

- (a) The effective stiffness of the modified rubber increased on average between 100% and 130% compared to that of the reference rubber.
- (b) The equivalent viscous damping ratio, β , of the modified rubber on average ranged between 0.15 and 0.2, that is, an increase of approximately 30% to 90% compared with the values obtained for the reference rubber.
- (c) Overall, the viscoelastic parameters of both rubber types exhibited a similar trend of variation with excitation frequency and shear strain amplitude. However, the modified rubber was found to be more sensitive than the reference rubber to the excitation frequency.

(3) Seismic response evaluation:

- (a) The seismic mitigation performance of the reference rubber was ineffective. This indicates that the inherent damping properties of CIIR rubber at room temperature are insufficient for effective performance as an elastomeric material in viscoelastic damper devices.
- (b) The modified rubber provided effective seismic mitigation by attenuating the cumulative modal energy of the structure, story drift, and internal forces of the structural members.

The results of this study suggest that the modified CIIR rubber with improved stiffness and damping properties is effective in seismic mitigation of structures.

Data Availability

The experimental data used to support the findings of this study are available from the corresponding author upon reasonable request.

Conflicts of Interest

The authors declare that they have no conflicts of interest.

Acknowledgments

The authors are grateful to Larzeh Badal Kar (LBK), Ltd. (<https://www.lbk.co.ir>), for the fabrication of the viscoelastic damper devices used in this study. The authors are also thankful to the Fatigue and Failure Laboratory, School of Mechanical, Aerospace and Maritime Engineering, Amir Kabir University of Technology, for their assistance in the laboratory tests of this study.

References

- [1] M. S. E. Nasab, Y.-Q. Guo, and J. Kim, "Seismic retrofit of a soft first-story building using viscoelastic dampers considering inherent uncertainties," *Journal of Building Engineering*, vol. 47, Article ID 103866, 2022.
- [2] F. Shang, W. Liu, H. Xu, and Q. Zhang, "Experimental investigation on amplified multilayer viscoelastic damper and vibration mitigation evaluation subjected to wind loads," *Journal of Building Engineering*, vol. 75, Article ID 106996, 2023.
- [3] H. A. Taleshian, A. M. Roshan, and J. V. Amiri, "Seismic pounding mitigation of asymmetric-plan buildings by using viscoelastic links," in *Structures*, Elsevier, Amsterdam, Netherlands, 2022.
- [4] F. Nikraves and H. Toopchi-Nezhad, "Application of viscoelastic tuned mass dampers in vibration mitigation of steel joist jack arch floor structures," *Shock and Vibration*, vol. 2022, Article ID 5196600, 13 pages, 2022.
- [5] Z. Shu, R. You, and Y. Zhou, "Viscoelastic materials for structural dampers: a review," *Construction and Building Materials*, vol. 342, Article ID 127955, 2022.
- [6] M. Achenbach and J. Duarte, "A finite element methodology to predict age-related mechanical properties and performance changes in rubber components," *Constitutive Models for Rubber*, pp. 59–70, AA Balkema Publishers, London, UK, 2003.
- [7] C. Christopoulos and A. Filiatrault, *Principles of Passive Supplemental Damping and Seismic*, IUSS Press, Pavia, Italy, 2006.
- [8] Z. He, F. Shi, Z. Lin, C. Zhang, Y. Zhou, and F. Zhao, "Experimental characterization on cyclic stability behavior of a high-damping viscoelastic damper," *Construction and Building Materials*, vol. 371, Article ID 130749, 2023.
- [9] C. Tsai, "Temperature effect of viscoelastic dampers during earthquakes," *Journal of Structural Engineering*, vol. 120, no. 2, pp. 394–409, 1994.
- [10] P. P. Hujare and A. D. Sahasrabudhe, "Experimental investigation of damping performance of viscoelastic material using constrained layer damping treatment," *Procedia Materials Science*, vol. 5, pp. 726–733, 2014.
- [11] L. Xia, C. Li, X. Zhang, J. Wang, H. Wu, and S. Guo, "Effect of chain length of polyisobutylene oligomers on the molecular motion modes of butyl rubber: damping property," *Polymer*, vol. 141, pp. 70–78, 2018.
- [12] M. Ghotb and H. Toopchi-Nezhad, "A feasibility study on pre-compressed partially bonded viscoelastic dampers," *Engineering Structures*, vol. 201, Article ID 109796, 2019.
- [13] W. Wei, P. Tan, Y. Yuan, and H. Zhu, "Experimental and analytical investigation of the influence of compressive load on rate-dependent high-damping rubber bearings," *Construction and Building Materials*, vol. 200, pp. 26–35, 2019.
- [14] Z.-D. Xu, Y. Yang, Y.-N. Zhu, and T. Ge, "Experimental study and mathematical modeling of viscoelastic dampers with wider temperature range based on blended rubber matrix," *Journal of Building Engineering*, vol. 70, Article ID 106414, 2023.
- [15] S. T. Jose, A. K. Anand, and R. Joseph, "EPDM/CIIR blends: improved mechanical properties through precuring," *Polymer Bulletin*, vol. 63, no. 1, pp. 135–146, 2009.

- [16] R. Suntako, "The rubber damper reinforced by modified silica fume (mSF) as an alternative reinforcing filler in rubber industry," *Journal of Polymer Research*, vol. 24, no. 8, pp. 131–137, 2017.
- [17] T. Ge, Z.-D. Xu, and F.-G. Yuan, "Development of viscoelastic damper based on NBR and organic small-molecule composites," *Journal of Materials in Civil Engineering*, vol. 34, no. 8, Article ID 4022192, 2022.
- [18] S. J. Therattil, A. A. Kuzhuppully, and J. Rani, *Compatibility Studies on sulphur Cured EPDM/CIIR Blends*, Iran Polymer and Petrochemical Institute, Tehran, Iran, 2008.
- [19] F. Zhang, G. He, K. Xu, H. Wu, S. Guo, and C. Zhang, "Damping mechanism and different modes of molecular motion through the glass transition of chlorinated butyl rubber and petroleum resin blends," *Journal of Applied Polymer Science*, vol. 131, no. 13, 2014.
- [20] C. Liu, J. Fan, and Y. Chen, "Design of regulable chlorobutyl rubber damping materials with high-damping value for a wide temperature range," *Polymer Testing*, vol. 79, Article ID 106003, 2019.
- [21] F. Zhang, G. He, K. Xu, H. Wu, and S. Guo, "The damping and flame-retardant properties of poly (vinyl chloride)/chlorinated butyl rubber multilayered composites," *Journal of Applied Polymer Science*, vol. 132, no. 2, 2015.
- [22] R. N. Capps and L. L. Beumel, *Dynamic Mechanical Testing: Application of Polymer Development to Constrained-Layer Damping*, ACS Publications, Washington, DC, USA, 1990.
- [23] X. Lu, X. Li, and M. Tian, "Preparation of high damping elastomer with broad temperature and frequency ranges based on ternary rubber blends," *Polymers for Advanced Technologies*, vol. 25, no. 1, pp. 21–28, 2014.
- [24] Z. Liu, Y. Wang, G. Huang, and J. Wu, "Damping characteristics of chlorobutyl rubber/poly (ethyl acrylate)/piezoelectric ceramic/carbon black composites," *Journal of Applied Polymer Science*, vol. 108, no. 6, pp. 3670–3676, 2008.
- [25] J. E. Mark, B. Erman, and M. Roland, *The Science and Technology of Rubber*, Academic Press, Oxford, UK, 2013.
- [26] K. Hanhi, M. Poikelispää, and H. Tirila, *Elastomeric Materials*, Tampere University of Technology, Tampere, Finland, 2020.
- [27] Astm, *D5026-15, Standard Test Method for Plastics: Dynamic Mechanical Properties: In Tension*, ASTM International, West Conshohocken, PA, USA, 2015.
- [28] F. Roshan-Tabari, *An improvement on the energy dissipation capability of chlorobutyl-based viscoelastic dampers*, Ph.D. thesis, Razi University, Kermanshah, Iran, 2023.
- [29] Asce, *Seismic Evaluation and Retrofit of Existing Buildings*, American Society of Civil Engineers, Reston, VA, USA, 2017.
- [30] M. Vašina, M. Pöschl, and P. Zádrapa, "Influence of rubber composition on mechanical properties," *Manufacturing Technology*, vol. 21, 2021.
- [31] Csi, *SAP2000 Integrated Software for Structural Analysis and Design*, Computers and Structures Inc, Berkeley, California, 2020.
- [32] H. G. Harris and G. Sabnis, *Structural Modeling and Experimental Techniques*, CRC Press, Boca Raton, FL, USA, 1999.
- [33] Asce, *Minimum Design Loads and Associated Criteria for Buildings and Other Structures*, American Society of Civil Engineers, Reston, VA, USA, 2022.